J Mol Model (2013) 19:4467–4475
DOI 10.1007/s00894-013-1938-1

ORIGINAL PAPER

Electrode materials for biphenyl-based rectification devices

Sweta Parashar · Pankaj Srivastava · Manisha Pattanaik

Received: 3 May 2013 / Accepted: 3 July 2013 / Published online: 9 August 2013

Abstract An ab initio approach was utilized to explore the electronic transport properties of 4′-thiolate-biphenyl-4-dithiocarboxylate (TBDT) sandwiched between two electrodes made of various materials X (X=Cu, Ag, and Au). Analysis of current–voltage (I–V) characteristics, rectification performance, transmission functions, and the projected density of states (PDOS) under various external voltage biases showed that the transport properties of these constructed systems are markedly impacted by the choice of electrode materials. Further, Cu electrodes yield the best rectifying behavior, followed by Ag and then Au electrodes. Interestingly, the rectification effects can be tuned by changing the torsion angle between the two phenyl rings, as well as by stretching the contact distances between the end group and the electrodes. For Cu, the maximum rectifying ratio increases by 37 % as the contact distance changes from 1.7 Å to 1.9 Å. This is due to an increase in coupling strength asymmetry between the molecule and the electrodes. Our findings are compared with the results reported for other systems. The present calculations are helpful not only for predicting the optimal electrode material for practical applications but also for achieving better control over rectifying performance in molecular devices.

Keywords Electrode materials · Rectification effects · Torsion angles · Stretching distances · First-principles calculations

S. Parashar · P. Srivastava (✉) · M. Pattanaik
Nanomaterials Research Group, Computational Nanoscience & Technology Laboratory (CNTL), ABV–Indian Institute of Information Technology & Management (ABV-IIITM), Gwalior 474015, India
e-mail: pankajs@iiitm.ac.in

Introduction

Molecular electron devices have attracted considerable attention owing to their great potential for practical applications in atomic-scale circuits. One of the many interesting challenges in this emerging field is to measure the electronic transport properties of a junction system containing a single molecule attached at each end to electrodes. A variety of experimental strategies have been utilized to probe electronic transport through single molecules in such metal–molecule–metal systems, including electrochemical [1], mechanically controllable break junction [2], self-assembled monolayer (SAM) [3], and scanning probe [4] techniques. The most striking properties of these systems are their single-electron characteristics [5], molecular rectification [6–8], negative differential resistance [9, 10], and electronic switching [11]. In particular, the molecular rectifier, initiated by Aviram and Ratner [6], is a basic functional element for building an electronic circuit. However, most of the research into such devices has focused on Au electrodes, since it is easy to prepare a clean Au surface using SAMs [12]. Moreover, from a practical application perspective, it is important for the junctions to be easily integrable as well as reliable and to have unique electrical characteristics. Hong et al. [13] reported that SAM-modified Ag electrodes are robust and reliable. Very recently, Kiguchi and coworkers [14] studied a system with Cu electrodes that utilized the mechanically controllable break junction technique, and found that electron-vibration interactions are responsible for conductance suppression when single hydrogen molecule bridging is present between Cu electrodes. It was also demonstrated that Cu electrodes are the best candidates for carbon nanocone rectification devices [15].

Understanding the electronic transport properties of a molecular device is an essential step in the further development of "bottom-up" molecule-based technologies, as the device properties of these systems cannot be determined by

simply combining the properties of the molecule and the electrode materials. Theoretical and experimental studies have demonstrated that the transport properties of a molecular device require systematic investigation of the system as a whole.Yaliraki and his co-workers [16], using a non-self-consistent method, investigated the transport properties of α,α′-xylyl-dithiol when it is used to bridge between two Au or Ag electrodes. They found that the conductance of Au(111) is five times higher than that of Ag(111). An early theoretical analysis of the dependence of the transport properties of biphenyl-based systems with symmetrical end groups on the electrode material is reported in [17]. Further, Taylor et al. [18] have highlighted the effect of the contact distance between the end group and the electrodes on electronic transport for junctions with symmetric end groups. Recently, it was observed that the torsion angle between the two phenyl rings significantly influences the transport properties of molecular devices [19–21]. Li and Kosov [22] reported that biphenyl-based systems with asymmetric end groups and Au electrodes display rectification behavior. However, there are many issues with asymmetric end groups, such as their physical mechanism, practical applications, and other related factors (e.g., effects of their spatial configurations, electrode materials, contact distances, etc.) that still need to be addressed. Motivated by this, we used Cu and Ag as electrodes to systematically investigate the transport properties in molecular devices with asymmetrical end groups using first-principles calculations. For comparison, we also performed such calculations for Au electrodes. Further, we also analyzed the effects of the torsion angle and contact distance on the transport properties when using different electrode materials. It turns out that the electrode material, torsion angle, and contact distance all have important influences on the coupling strength between molecule and electrodes, and thus on the rectification effects.

Model and computational methods

In the present work, all of the calculations were carried out using an ab initio package, ATK-VNL [23], which combines density functional theory (DFT) and the nonequilibrium Green's functions (NEGF) technique. This approach allowed us to simulate or explain the transport properties of two-probe systems that can be reasonably reproduced and verified using experimental results [24, 25]. Each two-probe system was divided into three regions: the left electrode, the right electrode, and the central scattering region. The central region also contained parts of the electrodes so that screening effects could be included in the calculations. The simulation method applied to such systems was as follows. Initially, the electronic structures of the left and right electrodes were calculated to obtain a self-consistent potential. This potential was shifted relative to each electrode by applying the bias voltage, which gave real-space boundary conditions for the Kohn–Sham (K-S) effective potential of the central device region. Using the Green's function of the central region, we obtained the density matrix and thereby the electron density. Utilizing the electron density, the DFT Hamiltonian matrix was then calculated using the above boundary conditions. This loop was repeated until self-consistency was achieved. Moreover, the current through the device was calculated using the Landauer–Büttiker formula [26, 27]:

$$I(V) = \frac{2e}{h}\int_{\mu_L}^{\mu_R} T(E, V_b)dE, \tag{1}$$

where μ_L and μ_R are the electrochemical potentials of the left and right electrodes which satisfy the relation $\mu_L - \mu_R = eV_b$. $[\mu_L, \mu_R]$ is the energy region of the transmission spectrum that contributes to the current integral, and is referred to as the bias window. $T(E, V_b)$ is the transmission coefficient at energy E and applied bias V_b. Based on eigenchannel decomposition of the conductance, this total transmission $T(E)$ was decomposed into non-mixing eigenchannels $T_n(E)$ [28] as

$$T(E) = \sum\nolimits_n T_n(E). \tag{2}$$

For the system at equilibrium, the conductance G was calculated via the transmission coefficient $T(E)$ at the Fermi energy E_f of the system:

$$G = \frac{2e^2}{h}T(E_f). \tag{3}$$

In our calculations, we used the Perdew–Zunger local density approximation (LDA) to describe the exchange-correlation functional [29]. Only valence electrons were considered, and the wavefunctions were expanded with localized numerical (pseudo) atomic orbitals (PAOs) [30]. In order to minimize computational effort and improve calculation precision, the valence electrons were expanded in a double-zeta plus polarization (DZP) basis set for metal atoms and a single-zeta plus polarization (SZP) basis set for other atoms. The convergence criterion in the NEGF/DFT self-consistent calculations was set to 10^{-5}, and the number of energy points used for the integration to calculate the current was 100. All of the geometries were optimized until the residual forces on each atom were less than 0.05 eV/Å. An energy cutoff value of 150 Ry was selected for the expansion of plane waves. To integrate the Brillouin zone, 1×1×150 k-points were used within the Monkhorst–Pack scheme. Further, we also performed calculations for 4×4×150 k-point sampling and found that it did not affect the important

features of the transmission spectra. A similar effect was also observed by Li and Kosov [22].

Results and discussion

Contact distances with the optimized system geometry

We considered a 4′-thiolate-biphenyl-4-dithiocarboxylate (TBDT) molecular junction system in which a dithiocarboxylate group was used on the left side while a thiol group was employed on the right side. Therefore, all of the systems constructed were asymmetric in geometry. Figure 1 shows the optimized junction geometries. In our study, we considered electrodes made of materials X (X=Cu, Ag, and Au), denoted by the wire boxes in the figure, and the molecule was connected to the X (111) electrodes with (3×3) periodicity. In order to validate the results using larger electrodes, we carried out test calculations using Cu(4×4) electrodes, and found no significant differences in their Cu(3×3) transmission spectra, and thus their derived characteristics. The same variations were expected for the Ag and Au electrodes, which were not computed in order to save computational effort. The S atom at each end was located at a hollow site, and therefore the relationship between the X–S bond length and the adsorption height was

$$d = \left[(h)^2 + 1/3(s)^2\right]^{1/2}, \tag{4}$$

where $s\left(=\text{lattice constant}/\sqrt{2}\right)$ is the X–X bond length and d is the X–S bond length in X (111) surface, while h is the distance between the X surface and the end-group atom, which is referred to as the adsorption height.

Table 1 shows the optimized contact distances L and r along with their corresponding transmissions $T(E_f)$ at the Fermi energy E_f of the electrode. Here, L is the optimized distance from the left electrode X surface to the left end group, and r is the distance from the right end group to the right X surface. For the left dithiocarboxylate group, L is the distance from the left electrode to the left atom S. It is evident from Table 1 that the transmissions $T(E_f)$ for molecular devices based on TBDT are much higher than the corresponding transmissions for those based on biphenyl dithiol (BPD) [17] and benzene dithiolate (BDT) [31, 32]. This is due to the fact that the left dithiocarboxylate group provides stronger coupling between the molecule and the electrodes than a thiol group [33], and thus high conductance at the Fermi level. Further, we also calculated the distance between electrodes (D) before and after optimizing junction geometries for all of the models considered, and found that the value of D was approximately the same (i.e., 24.84, 26.40, and 25.93 Å, respectively) for the Cu, Ag, and Au electrodes.

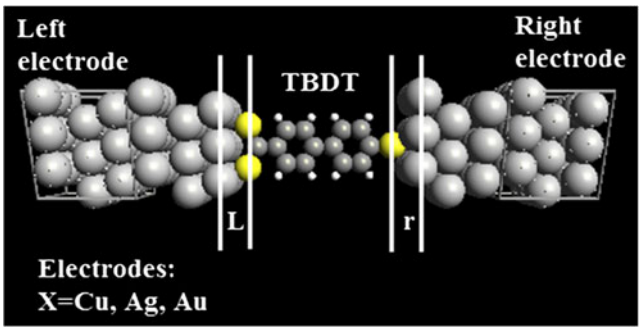

Fig. 1 Structure of the molecular device we constructed. TBDT was sandwiched between two X (X=Cu, Ag, Au) metal electrodes, with $L(r)$ referring to the optimized distance of the left (right) electrode from the left (right) end-group atom

Dependence on the electrode material

Using the optimized geometries, the self-consistently calculated current–voltage (I–V) characteristics for electrode materials X (X=Cu, Ag, and Au) in the bias range from −2 V to 2 V were derived, and are shown in Fig. 2a. Two important features of the evolution of the currents are clearly visible: (1) the magnitude of the current is higher for Au than for Cu and Ag, which indicates that the Au electrode is more conductive than the Cu and Ag electrodes, even at higher applied biases; and (2) all of the junctions have different voltage drops at the two metal–molecule contacts, thus resulting in asymmetric I–V characteristics. Moreover, the asymmetry in current is greatest for Cu, then Ag, and then Au. The asymmetries of the I–V curves for all of the models constructed are illustrated in Fig. 2b using the rectification ratio $R(|V_b|)$. $R(|V_b|)$ is defined as the ratio of the currents under positive and negative voltages for the same voltage magnitude, which was calculated via

$$R(|V_b|) = I(+|V_b|)/I(-|V_b|). \tag{5}$$

Cu clearly gives a stronger rectifying performance than Ag and Au, as shown in Fig. 2b. Table 2 lists the maximum rectification ratios $R_{max}(|V_b|)$ for the Cu, Ag, and Au electrodes of the considered junction systems, as well as the results available for other systems. It is apparent that the $R_{max}(|V_b|)$ values of the TBDT-based systems are higher than those for single-walled carbon nanocone (SWCN) [15] and oligo(phenylene ethynylene) (OPE) [34] devices. Moreover, the calculated $R_{max}(|V_b|)$ values of TBDT are in good agreement with other reported results [22]. The rectification ratio is a parameter that greatly influences the technological usefulness of a single-molecule device as a rectifier.

Further, the particular mechanism can be interpreted by analyzing the transmission spectrum. Figure 3 shows the

Table 1 Optimized contact distances L and r along with their corresponding transmissions $T(E_f)$

Electrode material X	Present calculations (X/TBDT/X)			Other calculations (X/BPD/X)		(X/BDT/X)		
	L (Å)	r (Å)	$T(E_f)$	r (Å)	$T(E_f)$	d (Å)	r (Å)	$T(E_f)$
Cu	1.815	1.589	0.2450	1.591[a]	0.0179[a]	2.30[b]	1.76	0.043[b]
Ag	2.054	1.760	0.1900	1.760[a]	0.0170[a]	2.49[b]	1.85	0.060[b]
Au	1.977	1.631	0.3000	1.631[a]	0.0525[a]	–	–	0.058[c]

[a] From [17]

[b] From [31]

[c] From [32]

transmission spectra $T(E)$ for electrodes X at 0 V. The average Fermi level, which is the average of the chemical potentials of the left and right electrodes, is set to zero. The two transmission peaks that appear near the Fermi level correspond to the highest occupied molecular orbital (HOMO) and the lowest unoccupied molecular orbital (LUMO), respectively. For all of the systems considered, the Fermi energy is close to the LUMO, which means that the electron transport is dominated by the LUMO. Furthermore, we can see that the transmission coefficient of the LUMO peak is much larger than that of the HOMO peak. In addition, the Au electrode has a taller LUMO peak than those of the Cu and Ag electrodes, so the magnitude of the current for Au is larger than those for the Cu and Ag electrodes. In order to further understand the transmission spectra, we calculated the density of states (DOS) of TBDT without electrodes, as shown in Fig. 4a, and found that the broad LUMO peak near the Fermi energy seen in the transmission spectra for all of the systems is in accord with the DOS, except that the peaks are shifted to higher energy, by about 0.5 eV. We also calculated the projected density of states (PDOS) for each of the systems constructed. Although the PDOS is slightly different for each material, the PDOS is similar to the transmission spectrum for each electrode. For example, the PDOSs for the Cu, Ag, and Au electrode materials (Fig. 4b) are similar to their transmission spectra (Fig. 3). The broad LUMO peak in the PDOS is shown more clearly in the inset of Fig. 4b.

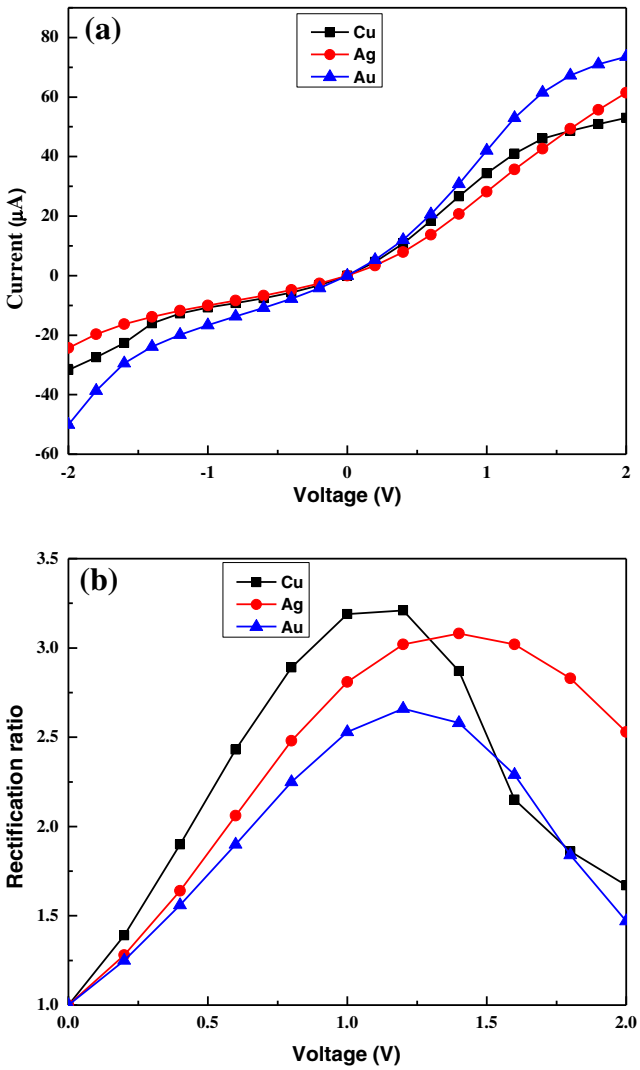

Fig. 2 **a** The current I and **b** the rectification ratio R as a function of applied bias for Cu, Ag, and Au electrodes

When the bias voltage is applied, the system is driven out of equilibrium and its electrode potential changes. Figure 5 shows the transmission spectra for different electrode materials X under voltages of ±1.2 and ±2.0 V. Since the current through the molecule sandwiched between two electrodes is given by the Landauer–Büttiker formula, as stated above, and the current is the integral of the transmission coefficient within the considered bias window, an analysis of the transmission spectra of Fig. 5 allows us to understand the I–V characteristics. For all of the systems, the left peak shifts toward the higher-energy orientation at a positive applied bias. However, the right peak shows the opposite behavior. This means that the HOMO peak follows the chemical

Table 2 The values of the maximum rectification ratios for Cu, Ag, and Au electrodes

	$R_{max}(\lvert V_b \rvert)$ at distance r (Å)			
	Present calculations	Other calculations		
Electrode material X	(X/TBDT/X)	(X/SWCNC/X)	(X/TBDT/X)	(Au/OPE/X)
Cu	3.2 (r=1.589)	1.6[a] (r=3.0)	–	–
Ag	3.1 (r=1.760)	1.55[a] (r=3.0)	–	2.4[c]
Au	2.7 (r=1.631)	2.0[a] (r=3.0)	2.8[b]	–

[a] From [15]
[b] From [22]
[c] From [34]

potential of the right electrode and the LUMO peak follows the chemical potential of the left electrode. Further, when the applied bias is less than 1.0 V, the shifting peaks cannot move into the bias window, even though the bias window increases, as the rate of expansion for the bias window is smaller than the shift in the transmission peaks. For Cu and Au, when the bias voltage is increased to +1.2 V, both the HOMO and the LUMO peaks enter the bias window [−0.6 eV, +0.6 eV] and produce maximum rectification ratios of 3.2 and 2.7, respectively. As a negative bias is applied and increased to 2.0 V, the HOMO peak enters the bias window. As a result, the current will increase slightly, so $R(\lvert V_b \rvert)$ will decrease. However, for Ag, the broad HOMO peak is far from the Fermi energy, and thus a bias of more than +1.2 V is required to shift both transmission peaks into the bias window. Therefore, $R_{max}(\lvert V_b \rvert)$ is obtained at an applied bias of +1.4 V. Thus, we can conclude that different rectification effects for Cu, Ag, and Au are observed due to changes in interfacial coupling.

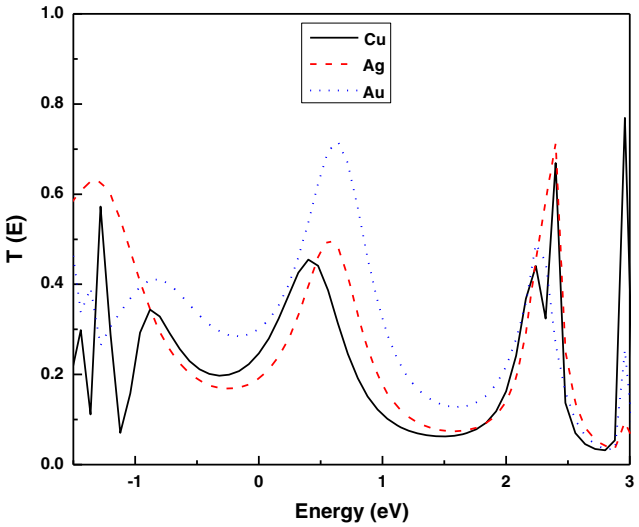

Fig. 3 Transmission spectra for the Cu, Ag, and Au electrodes at zero voltage

Torsion angle dependence

A complete understanding of the electronic transport mechanism associated with each electrode material required more

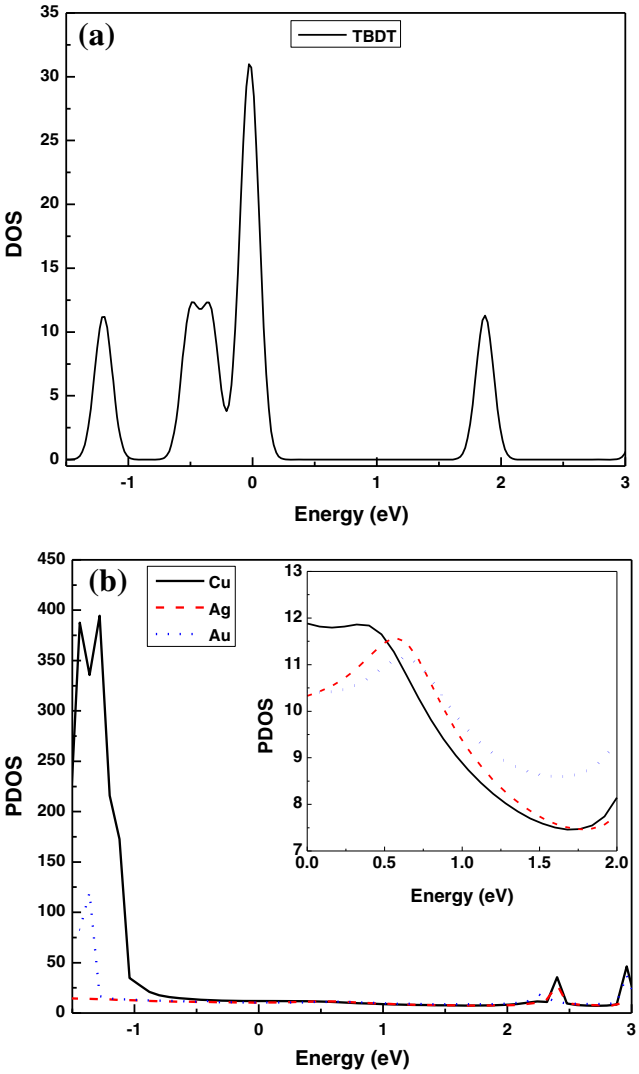

Fig. 4 **a** DOS of TBDT without electrodes. **b** Projected density of states for the Cu, Ag, and Au electrodes

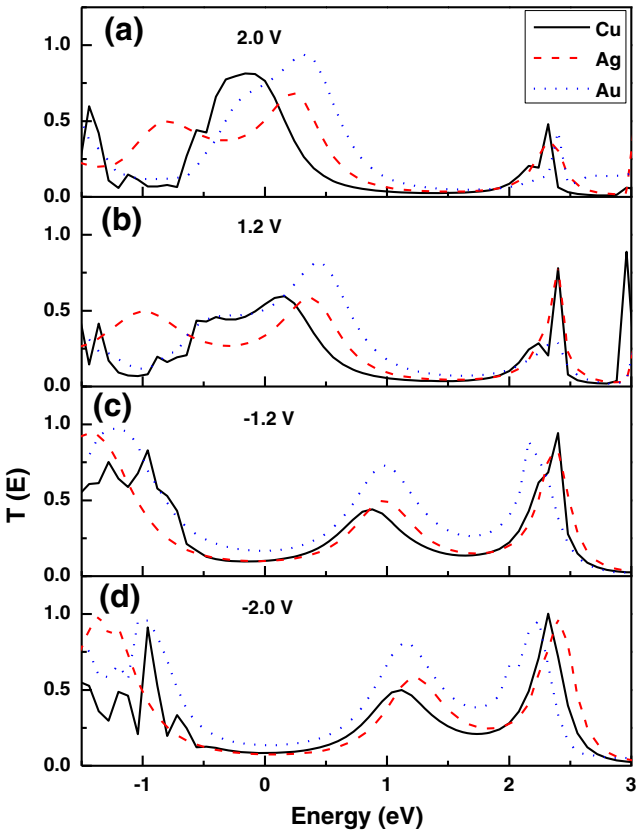

Fig. 5 Transmission spectra for the Cu, Ag, and Au electrodes under biases of ±1.2 and ±2.0 V

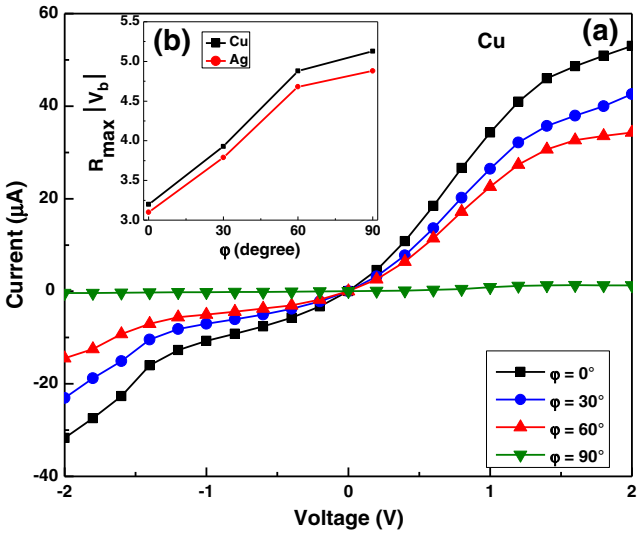

Fig. 6 **a** The current I as a function of the applied bias for Cu electrodes. **b** Maximum rectification ratio as a function of torsion angle φ for Cu and Ag electrodes

intensive investigation. Thus, we specifically studied the rectifying performance of X-TBDT-X molecular junctions at different torsion angles (φ=0º, 30º, 60º, and 90º) between two phenyl rings. As an example, Fig. 6 describes the I–V curve at different φ for the Cu electrodes, as it had the strongest rectifying performance among the different electrode materials X. From the figure, it is apparent that the current decreases as φ increases. The same trend was also observed for the Ag electrodes (not shown here). Further, the maximum rectification ratio $R_{max}(|V_b|)$ increases from 3.2 to 5.1 as the torsion angle φ is increased from 0 to 90º. This enhancement in $R_{max}(|V_b|)$ is due to an increase in the coupling asymmetry between the molecule and the electrodes [29]. For comparison, we also calculated $R_{max}(|V_b|)$ for Ag, as shown in Fig 6b. A similar increase in $R_{max}(|V_b|)$ (from 3.2 to 5.0) with increasing φ (from 0 to 90º) when using Au electrodes was noted by Wang et al. [21]. Therefore, the above results indicate that the increase in $R_{max}(|V_b|)$ with φ is nearly the same for all of the considered electrode materials X.

To further explore the obvious rectification effect, we plotted transmission spectra obtained under applied biases of 0 and ±1.2 V, as shown in Fig. 7. These show that when the torsion angle is small (i.e., 30º or 60º), the heights of the HOMO and LUMO peaks decrease with increasing φ, resulting in a smaller current. When φ becomes 90º, the peaks near the Fermi energy nearly disappear. Therefore, the current at φ=90º is very small, in accordance with the previous current analysis. The results reveal that the torsion angle between two phenyl rings plays an important role in

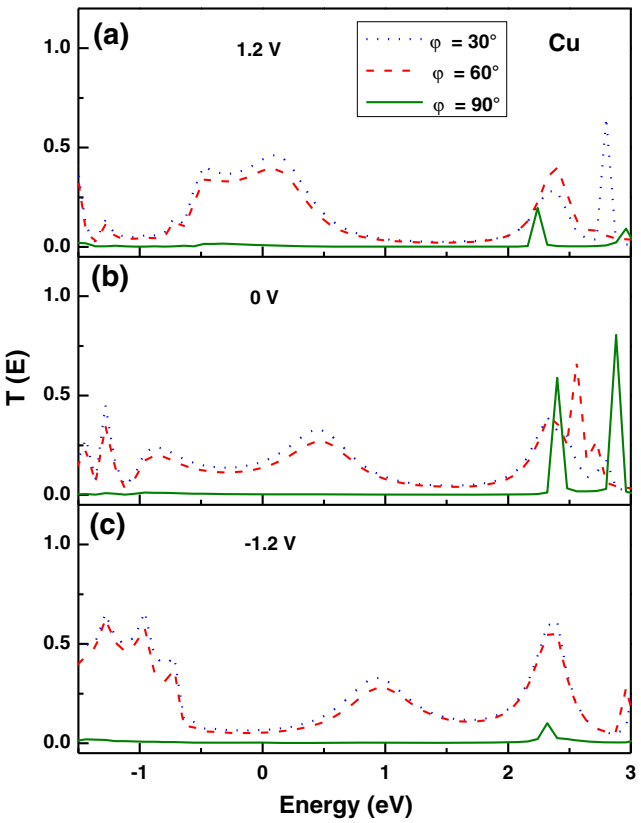

Fig. 7a–c Transmission spectra at different torsion angles φ for Cu electrodes under biases of **a** +1.2, **b** 0, and **c** −1.2 V

determining the rectifying performance of biphenyl-based molecular devices.

Dependence on the stretching distance

To study the dependence of the transport properties on the stretching distance, we first optimized the junction geometries by selecting distances between electrodes (D) of 25.34, 26.20, and 26.18 Å for the Cu, Ag, and Au electrodes, respectively. After optimization, L remained the same, as illustrated in Table 1, while r became 1.7 Å for each electrode X. Further, we stretched the junction by pulling the right electrode and then optimized the structures again. This process was repeated until one S–Cu bond was broken. Figure 8a shows the total change in energy (left axis) and the derivative of the energy (right axis) as a function of r for the TBDT junction using Cu electrodes. The change in total energy increases upon extension, whereas the derivative of the energy first increases and then drops near a distance r=1.9 Å. Similar behavior i.e. a decrease in the energy derivative upon the scission of one S–Au bond under normal and parallel stretching has also been observed by Wang et al. [35]. This indicates that one right S–Cu bond breaks at about r=1.9 Å. Figure 8a and b show relaxed TBDT junction geometries before (r=1.7 Å) and after the scission of one S–Cu bond on the right-hand side (r=1.9 Å).

For Cu, the I–V curve (Fig. 9) shows that the current continuously decreases with increasing r. Further, on increasing the distance r from 1.7 Å to 1.9 Å, the S–Cu bond weakens (Fig. 8(b)) which increases the left–right coupling strength asymmetry, and thus $R_{max}(|V_b|)$. From Fig. 9b, it is clear that $R_{max}(|V_b|)$ increases by 37 % when r changes from 1.7 Å to 1.9 Å. $R_{max}(|V_b|)$ values for the Cu, Ag, and Au electrodes are also presented in the figure, which shows that the increase in $R_{max}(|V_b|)$ for Cu is much higher than those for the Ag and Au electrodes. Our findings agree well with the theoretical results available for other systems [15], and confirm that the Cu electrode is the best substitute for Ag and Au electrodes in rectification devices.

In order to gain more insight into the microscopic mechanism for current asymmetry due to unequal coupling between the molecule and the electrode, we calculated the transmission spectra at 0 and ±1.2 V for the Cu electrodes, as shown in Fig. 10. For asymmetric contact geometries, stretching the distance r weakens the strength of coupling, leading to a higher potential barrier for electron transfer on the right contact. Neglecting the complicated electron process and assuming that the molecule's energy level is fixed, the electrostatic potentials of the left electrode μ_L and right electrode μ_R can be computed as [36]

$$\mu_L = E_f + \eta e V_b \tag{6a}$$

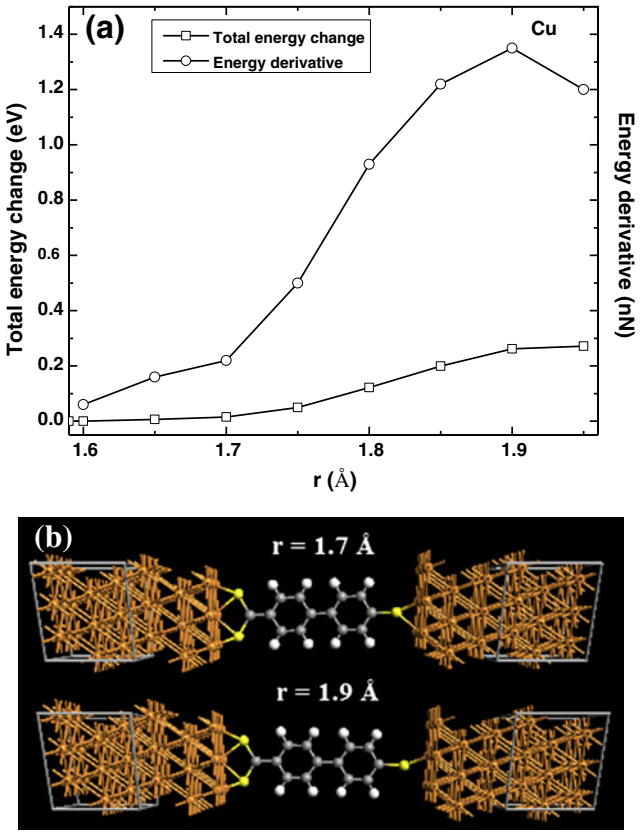

Fig. 8 **a** The total change in energy and the derivative of the energy as a function of the distance r for Cu electrodes. **b** Relaxed TBDT junction geometries before (r=1.7 Å) and after the scission of one S–Cu bond on the right-hand side (r=1.9 Å)

and

$$\mu_R = E_f - (1-\eta) e V_b, \tag{6b}$$

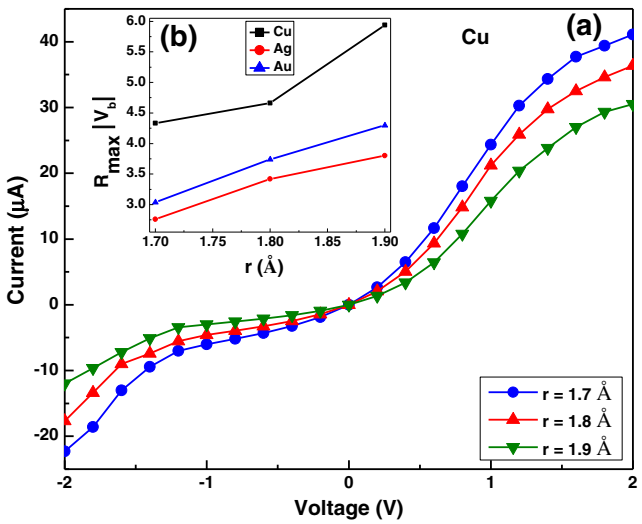

Fig. 9 **a** The current I as a function of the applied bias for Cu electrodes, and **b** the maximum rectification ratio as a function of the distance r for the Cu, Ag, and Au electrodes

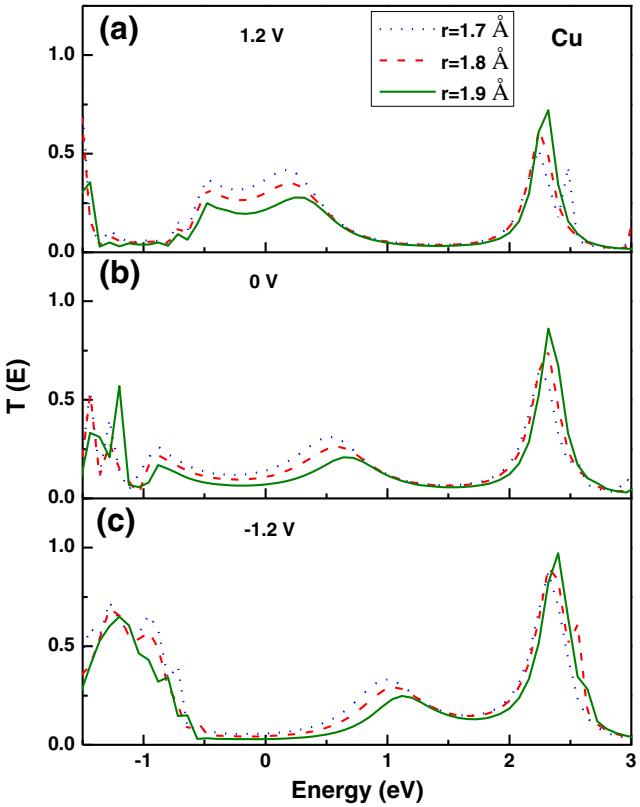

Fig. 10a–c Transmission spectra at different distances r for Cu electrodes under biases of **a** +1.2, **b** 0, and **c** −1.2 V

where e is the charge on an electron and $\eta<0.5$ for asymmetric contact ($\eta=0.5$ for symmetric contact). Therefore, when positive or negative bias is applied, μ_R moves further away from the Fermi energy E_f of the system (set as the molecule's energy level) than μ_L does. As a result, the heights of the transmission peaks near the Fermi energy decrease as r increases. Moreover, the transmission spectra shift to higher-energy orientations upon stretching the distance. Therefore, upon stretching the distance r, more than + 1.2 V is required for both the left HOMO and the right LUMO peaks to shift into the bias window and produce the maximum $R(|V_b|)$ in the molecular devices. The present calculation indicates that distance stretching is also an important factor when tuning rectification effects in TBDT devices.

Conclusions

We have investigated the dependence of the transport properties in biphenyl-based devices with asymmetric end groups on the electrode material X (X=Cu, Ag, and Au) using the non-equilibrium Green's function method combined with DFT. The results show that the evolution of I–V, the rectifying performance, transmission functions, and the projected density of states of TBDT are markedly impacted by the choice of electrode material. Further, Cu electrodes yield the best rectifying performance, followed by Ag and then Au electrodes. In addition, the rectification effects can be significantly improved by increasing the torsion angle between the two phenyl rings, as well as by stretching the contact distances between the end group and the electrodes. For Cu, the maximum rectifying ratio increases by 37 % as the contact distance is increased from 1.7 Å to 1.9 Å. This is due to an increase in coupling strength asymmetry between the molecule and the electrodes. The present calculation predicts that Cu electrodes are the best substitute for Au electrodes in the design of biphenyl-based rectification devices.

Acknowledgments The authors thank the Computational Nanoscience & Technology Laboratory (CNTL), Atal Bihari Vajpayee (ABV)–Indian Institute of Information Technology & Management, Gwalior (India) for providing the computational and infrastructural facilities.

References

1. Nitzan A, Ratner MA (2003) Electron transport in molecular wire junctions. Science 300:1384–1389. doi:10.1126/science.1081572
2. Halbritter A, Csonka S, Mihaly G, Jurdik E, Kolesnychenko OY, Shklyarevskii OI, Speller S, van Kempen H (2003) Transition from tunneling to direct contact in tungsten nanojunctions. Phys Rev B 68:035417. doi:10.1103/PhysRevB.68.035417
3. Ulman A (1996) Formation and structure of self-assembled monolayers. Chem Rev 96:1533–1554. doi:10.1021/cr9502357
4. Reed MA, Zhou C, Muller CJ, Burgin TP, Tour JM (1997) Conductance of a molecular junction. Science 278:25–2254. doi:10.1126/science.278.5336.252
5. Chen J, Reed MA, Rawlett AM, Tour JM (1999) Large on-off ratios and negative differential resistance in molecular electronic device. Science 286:1550–1552. doi:10.1126/science.286.5444.1550
6. Aviram A, Ratner MA (1974) Molecular rectifiers. Chem Phys Lett 29:277–283. doi:10.1016/0009-2614(74)85031-1, DOI:10.1016/0009-2614(74)85031-1
7. Metzger RM (2003) Unimolecular electrical rectifiers. Chem Rev 103:3803–3834. doi:10.1021/cr020413d
8. Zeng J, Chen KQ, He J, Zhang XJ, Sun CQ (2011) Edge hydrogenation-induced spin-filtering and rectifying behaviors in graphene nanoribbon heterojunctions. J Phys Chem C 115:25072–25076. doi:10.1021/jp208248v
9. Du Y, Pan H, Wang S, Wu T, Feng YP, Pan J, Wee ATS (2012) Symmetrical negative differential resistance behavior of a resistive switching device. ACS Nano 6:2517–2523. doi:10.1021/nn204907t
10. Zheng X, Lu W, Abtew TA, Meunier V, Bernholc J (2010) Negative differential resistance in C_{60}-based electronic devices. ACS Nano 4:7205–7210. doi:10.1021/nn101902r
11. Zeng J, Chen KQ, He J, Zhang XJ, Hu WP (2011) Rectifying and successive switch behaviors induced by weak intermolecular interaction. Org Electron 12:1606–1611. doi:10.1016/j.orgel.2011.06.010, DOI:10.1016/j.orgel.2011.06.010
12. Poirier GE, Pylant ED (1996) The self-assembly mechanism of alkanedithiols on Au(111). Science 272:1145–1148. doi:10.1126/science.272.5265.1145

13. Hong JP, Park AY, Lee S, Kang J, Shin N, Yoon DY (2008) Tuning of Ag work functions by self-assembled monolayers of aromatic thiols for an efficient hole injection for solution processed triisopropylsilylethynyl pentacene organic thin film transistors. Appl Phys Lett 92:143311. doi:10.1063/1.2907691
14. Matsushita R, Kaneko S, Nakazumi T, Kinguchi M (2011) Effect of metal–molecule contact on electron-vibration interaction in single hydrogen molecule junction. Phys Rev B 84:245412. doi:10.1103/PhysRevB.84.245412
15. Meng FX, Ming C, Zhuang J, Ning XJ (2013) Dependence of electronic rectification in carbon nanocone devices upon electrode materials. J Phys D Appl Phys 46:055309. doi:10.1088/0022-3727/46/5/055309
16. Yaliraki SN, Kemp M, Ratner MA (1999) Conductance of molecular wires: influence of molecule-electrode binding. J Am Chem Soc 121:3428–3434. doi:10.1021/ja982918k
17. Kondo H, Nara J, Kino H, Ohno T (2009) Transport properties of a biphenyl-based molecular junction system—the electrode metal dependence. J Phys Condens Matter 21:064220. doi:10.1088/0953-8984/21/6/064220
18. Taylor J, Brandbyge M, Stokbro K (2002) Theory of rectification in tour wires: the role of electrode coupling. Phys Rev Lett 89:138301. doi:10.1103/PhysRevLett.89.138301
19. Venkataraman L, Klare JE, Nuckolls C, Hybertsen MS, Steigerwald ML (2006) Dependence of single-molecule junction conductance on molecular conformation. Nature (London) 442:904–907. doi:10.1038/nature05037
20. Burkle M, Viljas JK, Vonlanthen D, Mishchenko A, Schon G, Mayor M, Wandlowski T, Pauly F (2012) Conductance mechanisms in biphenyl dithiol single-molecule junctions. Phys Rev B 85:075417. doi:10.1103/PhysRevB.85.075417
21. Wang LH, Guo Y, Tian CF, Song XP, Ding BJ (2010) Torsion angle dependence of the rectifying performance in molecular device with asymmetrical anchoring groups. Phys Lett A 374:4876–4879. doi:10.1016/j.physleta.2010.09.068
22. Li Z, Kosov DS (2006) Orbital interaction mechanisms of conductance enhancement and rectification by dithiocaboxylate anchoring group. J Phys Chem B 110:19116–19120. doi:10.1021/jp065120t
23. QuantumWise A/S (2011) AtomistixToolKit version 2011.2.8 (http://quantumwise.com)
24. Wang YF, Kroger J, Berndt R, Vazquez H, Brandbyge M, Paulsson M (2010) Atomic-scale control of electron transport through single molecules. Phys Rev Lett 104:176802. doi:10.1103/PhysRevLett.104.176802
25. Lindsay SM, Ratner MA (2007) Molecular transport junctions: clearing mists. Adv Mater 19:23–31. doi:10.1002/adma.200601140
26. Landauer R (1970) Electrical resistance of disordered one-dimensional lattices. Philos Mag 21:863–867. doi:10.1080/14786437008238472
27. Buttiker M (1986) Four-terminal phase-coherent conductance. Phys Rev Lett 57:1761. doi:10.1103/PhysRevLett57.1761
28. George CB, Ratner MA, Lambert JB (2009) Strong conductance in conformationally constrained oligosilane tunnel junctions. J Phys Chem A 113:3876–3880. doi:10.1021/jp809963r
29. Perdew JP, Zunger A (1981) Self-interaction correction to density-functional approximations for many-electron systems. Phys Rev B 23:5048–5079. doi:10.1103/PhysRevB.23.5048
30. Gonzalez MT, Wu S, Huber R, Wolen SJVD, Schonenberger C, Calame M (2006) Electrical conductance of molecular junctions by a robust statistical analysis. Nano Lett 6:2238–2242. doi:10.1021/nl061581e
31. Geng WT, Nara J, Ohno T (2004) Adsorption of benzene thiolate on the (111) surface of M (M=Pt, Ag, Cu) and the conductance of M/benzene dithiolate/M molecular junctions: a first-principles study. Thin Solid Films 464:379–383. doi:10.1016/j.tsf.2004.06.083
32. Nara J, Kino H, Kobayashi N, Tsukada, Ohno T (2003) Theoretical investigation of contact effects in conductance of single organic molecule. Thin Solid Films 438:221–224. doi:10.1016/S0040-6090(03)00774-0
33. Tivanski AV, He Y, Borguet E, Liu H, Walker GC, Waldeck DH (2005) Conjugated thiol linker for enhanced electrical conduction of gold-molecule contacts. J Phys Chem B 109:5398–5402. doi:10.1021/jp50022d
34. Pan JB, Zhang ZH, Ding KH, Deng XQ, Guo C (2011) Current rectification induced by asymmetrical electrode materials in a molecular device. Appl Phys Lett 98:092102. doi:10.1063/1.3556278
35. Wang GM, Sandberg WC, Kenny SD (2006) Density functional study of a typical thiol tethered on a gold surface: ruptures under normal or parallel stretch. Nanotechnology 17:4819–4824. doi:10.1088/0957-4484/17/19/006
36. Datta S, Tian W, Hong S, Reifenberger, Henderson JI, Kubiak CP (1997) Current–voltage characteristics of self-assembled monolayers by scanning tunneling microscopy. Phys Rev Lett 79:2530–2533. doi:10.1103/PhysRevLett.79.2530